Sea Ice Concentrations from Nimbus-7 SMMR and DMSP SSM/I-SSMIS Passive Microwave Data, Version 1

USER GUIDE

How to Cite These Data

As a condition of using these data, you must include a citation:

Cavalieri, D. J., C. L. Parkinson, P. Gloersen, and H. J. Zwally. 1996, updated yearly. *Sea Ice Concentrations from Nimbus-7 SMMR and DMSP SSM/I-SSMIS Passive Microwave Data, Version 1.* [Indicate subset used]. Boulder, Colorado USA. NASA National Snow and Ice Data Center Distributed Active Archive Center. https://doi.org/10.5067/8GQ8LZQVL0VL. [Date Accessed].

FOR QUESTIONS ABOUT THESE DATA, CONTACT NSIDC@NSIDC.ORG

FOR CURRENT INFORMATION, VISIT https://nsidc.org/data/NSIDC-0051

National Snow and Ice Data Center

TABLE OF CONTENTS

1 DATA DESCRIPTION 3
1.1.1 Accounting for Sensor Differences 3
1.1.2 Using these Data 4
1.2 Parameters 5
1.2.1 Parameter Description 5
1.2.2 Parameter Source 5
1.2.3 Parameter Range 5
1.3 File Information 6
1.3.1 Format 6
1.3.2 File Contents 6
1.3.3 Directory Structure 7
1.3.4 Naming Convention – Daily Files 7
1.3.5 Naming Convention – Monthly Files 8
1.3.6 File Size 8
1.4 Spatial Information 9
1.4.1 Coverage 9
1.4.2 Resolution 9
1.4.3 Projection and Grid Description 9
1.5 Temporal Information 10
1.5.1 Coverage 10
1.5.2 Resolution 10
2 DATA ACQUISITION AND PROCESSING 10
2.1 Background 10
2.2 Acquisition 10
2.2.1 SMMR 11
2.2.2 SSM/I and SSMIS 11
2.3 Derivation Techniques and Algorythms 11
2.4 Processing 12
2.4.1 Platform and Sensor Differences 12
2.4.2 Land-to-Ocean Spillover and Residual Weather-Related Effects 14
2.4.3 Manual Quality Control 17
2.4.4 Filling Data Gaps 17
2.4.5 Monthly Data Generation 18
2.5 Quality, Errors, and Limitations 18
2.5.1 Data Validation by Source 18
2.5.2 Confidence Level/Accuracy Judgment 19
2.5.3 Data Verification by Data Center 19
2.5.4 File Errors 21
2.5.5 Sea Ice Pixel Correction 23

2.6 Instrumentation 24
2.6.1 Description 24
2.6.2 Trajectory and Attitude 24
3 SOFTWARE AND TOOLS 25
4 VERSION HISTORY 26
5 RELATED DATA COLLECTIONS 26
6 ACKNOWLEDGMENTS 27
7 REFERENCES 27
8 DOCUMENT INFORMATION 29
8.1 Publication Date 29
8.2 Date Last Updated 29

1 DATA DESCRIPTION

This data set is generated from brightness temperature data derived from the following sensors: The Nimbus-7 Scanning Multichannel Microwave Radiometer (SMMR), the Defense Meteorological Satellite Program (DMSP) -F8, -F11 and -F13 Special Sensor Microwave/Imagers (SSM/Is), and the DMSP-F17 Special Sensor Microwave Imager/Sounder (SSMIS). The data are provided in the polar stereographic projection at a grid cell size of 25 x 25 km.

This product is designed to provide a consistent time series of sea ice concentrations (the fraction, or percentage, of ocean area covered by sea ice) spanning the coverage of several passive microwave instruments. To aid in this goal, sea ice algorithm coefficients are changed to reduce differences in sea ice extent and area as estimated using the SMMR and SSM/I sensors. The data are generated using the NASA Team algorithm developed by the Oceans and Ice Branch, Laboratory for Hydrospheric Processes at NASA Goddard Space Flight Center (GSFC).

These data include gridded daily (every other day for SMMR data) and monthly averaged sea ice concentrations for both the north and south polar regions. The data are produced at GSFC about once per year, with roughly a one-year latency, and include data since 26 October 1978. Data are produced from SMMR brightness temperature data processed at NASA GSFC and from SSM/I and SSMIS brightness temperature data processed at the National Snow and Ice Data Center (NSIDC).

Data are scaled and stored as one-byte integers in flat binary arrays. For each data file, a corresponding PNG browse image file is provided.

1.1.1 Accounting for Sensor Differences

The goal of this data set is to provide a long term, consistent sea ice concentration product in which sea ice extent and area differences between the sensors are reduced and could serve as a baseline for future measurements. To achieve this, it is necessary to address differences between the SMMR and the DMSP-F8, -F11, and -F13 SSM/I sensors, as well as the DMSP-F17 SSMIS sensor. This document describes the basic characteristics of the SMMR, SSM/I, and SSMIS platforms and summarizes the problems encountered when deriving sea ice concentrations from brightness temperatures measured by sensors with different frequencies, different footprint sizes, different visit times, and different calibrations. A major obstacle to resolving these differences is the lack of sufficient overlapping data from sequential sensors. The techniques employed to solve these problems, or at least reduce their impacts, include:

- Mapping the sensor data onto a common grid
- Applying a new land mask
- Addressing instrument drift
- Adjusting for land-to-ocean spillover

- Replacement of bad data
- Inter-sensor corrections made to reduce remaining measurement differences

Basic limitations also arise from the sensor resolution, temporal coverage, and algorithm assumptions and characteristics. The NASA Team algorithm is not designed to provide ice concentration for fresh-water ice (for example, lake and river ice). The filtering used to remove land-to-ocean spillover may affect the area of some open water features within the ice pack near coasts (coastal polynyas).

1.1.2 Using these Data

Potential applications for these sea ice concentration data include:

- Monitoring the distribution, extent, and area of the Arctic and Antarctic sea ice cover
- Identifying and monitoring large, persistent open water areas surrounded by sea ice (polynyas)
- Analyses of regional and global trends in sea ice cover
- Validation of sea ice models and climate models
- Analysis of sea ice/ocean and sea ice/atmosphere interactions

Users should be aware that the ice concentration maps were derived from algorithms that were "tuned" to minimize the differences in ice extent and ice covered area during the overlap periods when transitioning from one instrument to the next (overlap from SMMR to DMSP-F8 SSM/I, from DMSP-F8 to -F11 SSM/I, from DMSP-F11 to -F13 SSM/I, and from DMSP-F13 SSM/I to DMSP-F17 SSMIS). This does not mean that the ice concentrations themselves are well matched. See the Data Verification by Data Center section of this document for a summary of ice extent and ice covered area differences during the overlap periods.

It is also important to know that SMMR and SSM/I-SSMIS have different data gaps at the North Pole due to orbital differences. Therefore, any time series of parameters, such as ice extent and ice covered area, need to take these differences into account. A pole mask is provided for this purpose. See the polar stereographic tools webpage for masks and overlays details.

Particular care is needed to interpret the sea ice concentrations during summer when melt is present, and in regions where new sea ice makes up a substantial part of the sea ice cover. Some residual errors remain due to weather effects and mixing of ocean and land area within the sensor field of view, or FOV, and due to sensor differences.

It is recommended that sea ice extent and area be computed from daily maps of ice concentrations that are then used to compute monthly averages of those parameters. Computations of sea ice extents and sea ice areas should not be made from the monthly-averaged ice concentration maps because that may result in a biased time series.

1.2 Parameters

1.2.1 Parameter Description

Sea ice concentration represents an areal coverage of sea ice. For a given grid cell, the parameter provides an estimate of the fractional amount of sea ice covering that cell, with the remainder of the area consisting of open ocean. Land areas are coded with a land mask value.

1.2.2 Parameter Source

Data sources are Nimbus-7 SMMR, DMSP-F8, -F11 and -F13 SSM/I instruments, and the DMSP-F17 SSMIS instrument.

1.2.3 Parameter Range

Data are stored as one-byte integers representing sea ice concentration values. The sea ice concentration data are packed into byte format by multiplying the derived fractional sea ice concentration floating-point values (ranging from 0.0 to 1.0) by a scaling factor of 250. For example, a sea ice concentration value of 0.0 (0%) maps to a stored one-byte integer value of 0, and a sea ice concentration value of 1.0 (100%) maps to a stored one-byte integer value of 250. To convert to the fractional parameter range of 0.0 to 1.0, divide the scaled data in the file by 250. To convert to percentage values (0% to 100%), divide the scaled data in the file by 2.5.

Data files may contain integers from 0 to 255, as described in Table 1.

Table 1. Description of Data Values

Data Value	Description
0 - 250	Sea ice concentration (fractional coverage scaled by 250)
251	Circular mask used in the Arctic to cover the irregularly-shaped data gap around the pole (caused by the orbit inclination and instrument swath)
252	Unused
253	Coastlines
254	Superimposed land mask
255	Missing data

1.3 File Information

1.3.1 Format

Data are provided in scaled, unsigned flat binary files (.bin) with one byte per pixel; they have no byte order or endianness. Data are stored as one-byte integers representing scaled sea ice concentration values.

For each data file, a corresponding browse image file in PNG format is also provided.

Extensible Markup Language (.xml) files with associated metadata are also provided.

1.3.2 File Contents

The file format consists of a 300-byte descriptive header followed by a two-dimensional array of one-byte values containing the data. The file header is composed of:

- a 21-element array of 6-byte character strings that contain information such as polar stereographic grid characteristics
- a 24-byte character string containing the file name
- a 80-character string containing an optional image title
- a 70-byte character string containing ancillary information such as data origin, data set creation date, etc.

For compatibility with ANSI C, IDL, and other languages, character strings are terminated with a NULL byte.

The file header can be accessed in a variety of ways. For example, it can be treated as a simple sequence of bytes containing ASCII character strings or as a complex data structure of arrays. Table 2 describes the file header.

Table 2. File Header Description

Bytes	Description
1-6	Missing data integer value
7-12	Number of columns in polar stereographic grid
13-18	Number of rows in polar stereographic grid
19-24	Unused/internal
25-30	Latitude enclosed by polar stereographic grid
31-36	Greenwich orientation of polar stereographic grid
37-42	Unused/internal
43-48	J-coordinate of the grid intersection at the pole

Bytes	Description
49-54	I-coordinate of the grid intersection at the pole
55-60	Five-character instrument descriptor (SMMR, SSM/I, SSMIS)
61-66	Two descriptors of two characters each that describe the data; (for example, 07 cn = Nimbus-7 ice concentration)
67-72	Starting Julian day of grid data
73-78	Starting hour of grid data (if available)
79-84	Starting minute of grid data (if available)
85-90	Ending Julian day of grid data
91-96	Ending hour of grid data (if available)
97-102	Ending minute of grid data (if available)
103-108	Year of grid data
109-114	Julian day of grid data
115-120	Three-digit channel descriptor (000 for ice concentrations)
121-126	Integer scaling factor
127-150	24-character file name (without file-name extension)
151-230	80-character image title
231-300	70-character data information (creation date, data source, etc.)

The data can be read with image processing software by specifying a 300-byte header, with an image size of 304 columns x 448 rows for Arctic data and 316 columns x 332 rows for Antarctic data. For example, in a high-level programming language or image processing software, declare a 300-byte array for the header and a 304 x 448 Arctic image array. Read the 300-byte header array first, then read the image array.

1.3.3 Directory Structure

Data are available for download at: https://n5eil01u.ecs.nsidc.org/PM/NSIDC-0051.001/

Within the download directory, folders are organized by date in YYYY.MM.DD format, for example /1993.08.01/. Each folder contains the sea ice concentration data files, browse images, and associated metadata for both the Northern and Southern Hemispheres. Monthly files are also included in the folder for the first day of each month.

1.3.4 Naming Convention – Daily Files

Data files are named according to the following conventions and as described in Table 3:

```
nt_YYYYMMDD_SSS_vVV_R.ext
```

Table 3. Daily Data File Naming Convention

Variable	Description
nt	Indicates this was created with the NASA Team algorithm
YYYY	Four-digit year
MM	Two-digit month
DD	Two-digit day
SSS	Sensor (n07 for Nimbus-7 SMMR; f08, f11, or f13 for DMSP-F8, -F11 or -F13 SSM/I; f17 for DMSP-F17 SSMIS)
VV	Data version number (for example, 01)
R	Region (n = north; s = south)
.ext	File extension (.bin = binary, .png = PNG image)

Example File Name: nt_20140131_f17_v01_n.bin

1.3.5 Naming Convention – Monthly Files

Data files are named according to the following conventions and as described in Table 4:

nt_YYYYMM_SSS_vVV_R.ext

Table 4. Monthly Data File Naming Convention

Variable	Description
nt	Indicates this was created with the NASA Team algorithm
YYYY	Four-digit year
MM	Two-digit month
SSS	Sensor (n07 for Nimbus-7 SMMR; f08, f11, or f13 for DMSP-F8, -F11 or -F13 SSM/I; f17 for DMSP-F17 SSMIS)
VV	Data version number (for example, 01)
R	Region (n = north; s = south)
.ext	File extension (.bin = binary, .png = PNG image)

Example File Name: nt_201401_f17_v01_n.bin

1.3.6 File Size

Data file size varies by region:

- North: 136492 bytes
- South: 105212 bytes

1.4 Spatial Information

1.4.1 Coverage

Data set coverage includes the polar regions, as defined by the Polar Stereographic Projections and Grids spatial coverage map.

Each of the three instruments provide global coverage except for a circular sector centered over the North Pole. These sectors are never measured due to orbit inclination of the satellite. Table 5 shows the sizes and latitudes of each of the pole holes.

NOTE: The SSMIS pole hole was implemented in March 2015 and applied to all data from January 2008 to present. Even though SSMIS data begin in January 2007, this product does not start using the SSMIS pole hole mask until January 2008 to allow for comparison analysis with SSM/I during the transition from SSM/I to SSMIS data in 2007.

Table 5. Pole Hole Sizes and Dates by Mask

Pole Hole Mask Name	Pole Hole Area (million km2)	Pole Hole Radius (km)	Latitude	Dates Used
SSMIS Pole Hole Mask	0.029	94	89.18° N	January 2008 to present
SSM/I Pole Hole Mask	0.31	311	87.2° N	July 1987 through December 2007
SMMR Pole Hole Mask	1.19	611	84.5° N	November 1978 through June 1987

1.4.2 Resolution

The spatial resolution for this data set is 25 km.

1.4.3 Projection and Grid Description

The sea ice concentration data are displayed in polar stereographic projection. For more information, see Polar Stereographic Projections and Grids. The grid size varies depending on the region, as shown in Table 6.

Table 6. Regional Grid Size

Region	Columns	Rows
North	304	448
South	316	332

1.5 Temporal Information

1.5.1 Coverage

Data are from 26 October 1978 through 31 December 2021. See the "Acquisition" section of this document for dates by instrument and platform.

1.5.2 Resolution

The SMMR instrument scanner operated only on alternate days, due to spacecraft power limitations. Therefore, SMMR data were only collected every other day. Typically, there are at least 14 days of coverage per month, although there are major data gaps in August of 1982 (04, 08, and 16 August 1982), and in August of 1984 (13 through 23 August 1984) for both polar regions.

SSM/I data were collected daily and SSMIS data continue to be collected daily. A major data gap in the SSM/I data exists from 03 December 1987 to 13 January 1988.

Sea ice concentrations are provided for each day of data and also as monthly means. The monthly means are generated by averaging all the available daily files for each individual month, excluding pixels of missing data. Refer to the Monthly Data Generation section of this document for more information.

2 DATA ACQUISITION AND PROCESSING

2.1 Background

The SMMR, SSM/I, and SSMIS instruments are microwave radiometers that sense emitted microwave radiation. This radiation is affected by surface and atmospheric conditions, and thus provides a range of geophysical information.

2.2 Acquisition

The combined SMMR, SSM/I, and SSMIS sea ice concentration time series is produced from brightness temperatures obtained from GSFC and NSIDC. The four sets of satellite data currently used to create this data stream and the time periods for which the data are available are shown in Table 7.

Table 7. Time Periods for Data

Platform and Instrument	Time Period
Nimbus-7 SMMR	26 October 1978 through 20 August 1987
DMSP-F8 SSM/I	21 August 1987 through 18 December 1991
DMSP-F11 SSM/I	19 December 1991 through 29 September 1995
DMSP-F13 SSM/I	30 September 1995 through 31 December 2007
DMSP-F17 SSMIS	01 January 2008 through 31 December 2021

2.2.1 SMMR

Sea ice concentrations were processed by GSFC using SMMR brightness temperatures. The SMMR brightness temperatures were processed and quality checked at GSFC (Gloersen et al. 1992).

2.2.2 SSM/I and SSMIS

SSM/I and SSMIS brightness temperature data used to create this sea ice concentration time series are distributed by NSIDC. Processing of DMSP-F17 SSMIS brightness temperatures is ongoing.

2.3 Derivation Techniques and Algorythms

This section is extracted from NASA Technical Memorandum 104647 (Cavalieri et al., 1997).

Sea ice concentrations for this data set were produced using a revised NASA Team algorithm that uses a different set of tie points and a different weather filter than the original NASA Team algorithm; see the Descriptions of and Differences between the NASA Team and Bootstrap Algorithms FAQ for a description of the original algorithm. The NASA Technical Memorandum 104647 (Cavalieri et al., 1997) includes information about differences, such as tie points, between the original algorithm and the revised NASA Team algorithm. In addition, the NASA Team algorithm uses different channels of the SMMR and the SSM/I-SSMIS brightness temperature data (Table 8).

Table 8. SMMR and SSM/I-SSMIS Brightness Temperature Channels

Instrument	Channels
SMMR	• Vertically and horizontally polarized (v-pol and h-pol) 18.0 GHz • V-pol 37.0 GHz
SSM/I	• V-pol and h-pol 19.3 GHz • V-pol 37.0 GHz

Instrument	Channels
SSMIS	• V-pol and h-pol 19.3 GHz • V-pol 37.0 GHz

The weather filter used for the SMMR (Gloersen and Cavalieri, 1986) was found to be inadequate for the SSM/I due to the SSM/I's use of the 19.3 GHz channel (which is further up on the shoulder of the water vapor line at 22.2 GHz) rather than the 18.0 GHz channel. A different weather filter is used to reduce spurious sea ice concentrations from SSM/I that result from the presence of atmospheric water vapor, non-precipitating cloud liquid water, rain, and sea surface roughening by surface winds. This filter is a combination of the SSM/I 37.0 and 19.3 GHz channels, which effectively eliminates most of the spurious sea ice concentration measurements resulting from wind-roughening of the ocean surface, cloud liquid water, and rainfall. Another filter that is based on the 19.3 and 22.2 GHz channels is also used. The rationale behind combining the 19.3 and 22.2 GHz channels is based on the sensitivity of the 22.2 GHz to water vapor and on the need to minimize the effect of ice temperature variations at the ice edge.

2.4 Processing

2.4.1 Platform and Sensor Differences

Comparisons of sea ice concentrations calculated for each sensor during overlap periods using published algorithm tie points reveal significant differences. These may result from differences in sensor and orbital characteristics, differences in observation times (and therefore tidal effects), and/or differences in algorithm coefficients. Sensor and orbital characteristic differences for the Nimbus-7 SMMR and DMSP-F8 SSM/I include antenna beam width, channel frequency, spacecraft altitude, ascending node time, and angle of incidence. In addition, the sea ice algorithm tie points are significantly different. The DMSP sensors also differ in ascending node time, altitude, and angle of incidence. Because the visit times of the DMSP satellites occur during different phases of the diurnal cycle, tidal effects may result in differences in the sea ice distribution. GSFC presumes that any such effects are mitigated by the correction scheme described below. The *Comparison of Orbital Parameters* table in the Instrument section of this document summarizes sensor and orbital characteristic differences. The GSFC processing attempts to accommodate for these differences in each pair of sensors by employing a set of algorithm tie points determined through linear relationships between the observed brightness temperatures during the overlap periods.

2.4.1.1 Nimbus-7 SMMR to DMSP-F8 SSM/I Transition

Daily brightness temperature maps from the Nimbus-7 SMMR and from the DMSP-F8 SSM/I during their period of overlap, 09 July to 20 August 1987, were compared for both the Arctic and Antarctic. Unfortunately, there were only 22 days of common coverage. A linear, least-squares

best-fit of the cumulative data was obtained for each of the corresponding channels. For the purpose of eliminating spurious brightness temperatures resulting from residual land spillover effects, an Arctic land mask that expanded three to four pixels out from the original land mask was used in the determination of the best fit between the two data streams.

The eliminated pixels represent only a very small fraction of the total number of sea ice concentration pixels, but eliminating them helps considerably in reducing the outliers on the scatter plots. These linear relations were used to generate a set of SSM/I tie points that are consistent with the original SMMR sea ice algorithm tie points (Gloersen et al., 1992). The published DMSP-F8 SSM/I tie points (Cavalieri et al., 1992) were not used. In addition to using these transformations, the DMSP-F8 SSM/I open water tie points were subjectively tuned to help minimize the differences between the SMMR and DMSP-F8 SSM/I sea ice extent and area during the overlap period. In all cases, except for the Antarctic DMSP-F8 SSM/I values, the tuned amount is within one standard error of estimate. GSFC suspects the reason for the larger tuned values results from greater weather effects during the overlap period.

For more information on the regression coefficients and revised tie points, see the NASA Technical Memorandum 104647 (Cavalieri et al., 1997).

2.4.1.2 DMSP-F8 to DMSP-F11 SSM/I Transition

The transition period from DMSP-F8 to -F11 includes only 16 days of good data overlap, from 03 to 18 December 1991. The DMSP-F11 SSM/I open water tie points were also tuned to help reduce differences in sea ice extent and area as was done with the DMSP-F8 SSM/I values. A further adjustment to the Antarctic 37V sea ice type-B F11 tie point was also made to reduce the sea ice area difference. In this case, the amount of tuning needed to reduce the sea ice extent and area differences between the DMSP-F8 and -F11 values is well within one standard error of estimate.

2.4.1.3 DMSP-F11 to DMSP-F13 SSM/I Transition

The effects of changing from the DMSP-F11 to the -F13 satellite were examined for a 5-month overlap period, from 5 May 1995 through 30 September 1995. Generally, in terms of hemispheric averages of mean ice concentration, the biases introduced by the transition are slight and not statistically significant; however, in some regions relatively large and significant differences are seen. In addition, differences in sea ice extent and total ice covered area between the two platforms were found to be statistically significant. For more information, please see the NSIDC Special Report 5: An Intercomparison of DMSP F11- and F13-derived Sea Ice Products (Stroeve, Li, & Maslanik, 1997).

2.4.1.4 DMSP-F13 SSM/I to DMSP-F17 SSMIS Transition

The effects of changing from the DMSP-F13 SSM/I to the -F17 SSMIS were examined for a 12-month overlap period, from 01 January 2007 to 31 December 2007. Differences in sea ice extent and total ice covered area between the two platforms and instruments were found to be statistically significant, though fairly similar when compared with previous intersensor calibrations conducted for this time series (Cavalieri et al., 1999). Earlier intersensor calibrations, however, were limited by relatively short periods of sensor overlap (such as sixteen days) and could thus account for less agreement with this transition (Cavalieri et al., 2012). In addition, earlier agreement may be due to the subjective tuning of some tie-points that was required in past intercalibrations (Cavalieri et al., 1999).

2.4.2 Land-to-Ocean Spillover and Residual Weather-Related Effects

The next step in preparing the data is the correction for land-to-ocean spillover, often referred to as "land contamination," and residual weather-related effects. While these steps eliminate much of the land-to-ocean spillover and weather effects over open ocean, these problems are not entirely removed. See the section Data Verification by Data Center for additional comments.

2.4.2.1 Land-to-Ocean Spillover

Land-to-ocean spillover refers to the issue of the blurring of sharp contrasts in brightness temperature, such as those that exist between land and ocean, due to the relatively coarse width of the sensor antenna pattern. This problem is of concern because it results in false sea ice signals along coastlines because both land and sea ice have much higher brightness temperatures than ocean. The method used to reduce the spillover is an extension of the method employed for the single-channel Nimbus-5 Electrically Scanning Microwave Radiometer (ESMR) data in Parkinson et al. (1987). Figure 1a illustrates the effect of the coarse resolution of the microwave antenna on a coastline resulting in false sea ice signals in the vicinity of the coast, and Figure 1b shows the seven-by-seven array used in the procedure to reduce the land-to-ocean spillover effect. The rationale behind the approach is that a minimum observed sea ice concentration in the vicinity of coastlines where no sea ice remains offshore, which is generally seen in late summer, is probably the result of land spillover; so it is subtracted from the image. To reduce the error of subtracting sea ice in areas of actual sea ice cover, the technique searches for and requires the presence of open water in the vicinity of the image pixel to be corrected.

Land-to-ocean spillover was reduced by the following three-step procedure:

1. A matrix M was created covering the entire grid and identifying each pixel as land, shore, near-shore, offshore, or non-coastal ocean. The identification of land pixels was straightforward; they were obtained from the land/sea mask (see NASA Technical

Memorandum 104625 [Martino et al., 1995]). The identification of shore, near-shore, and offshore pixels was based on the scheme shown in Figure 1b, where the pixel to be identified is labeled I,J. This pixel is considered a *shore* pixel if any pixel adjacent to it is land, a *near-shore* pixel if none of the A pixels are land but at least one of the B pixels is land, and an *offshore* pixel if none of the A or B pixels are land but at least one of the C pixels is land. All other ocean pixels are considered *non-coastal ocean*. This matrix M is created once and used throughout the data set.

2. A matrix CMIN, to represent minimum sea ice concentrations on a pixel-by-pixel basis throughout the entire grid, was created for each instrument type. CMIN was created by first constructing a matrix P containing the minimum monthly average sea ice concentrations throughout a given year, then adjusting that matrix at offshore, near-shore, and shore pixels. In the case of SMMR, 1984 monthly data were used, whereas in the case of SSM/I, 1992 monthly data were used. In both cases, the adjustments were as follows: (a) at offshore pixels, any P values exceeding 20 percent were reduced to 20 percent; (b) at near-shore pixels, any P values exceeding 40 percent were reduced to 40 percent; and (c) at shore pixels, any P values exceeding 60% were reduced to 60 percent. The CMIN matrix was created once for SMMR and once for SSM/I, then used throughout the data set.
3. The daily sea ice concentration matrices were adjusted at any offshore, near-shore, and shore pixels in the vicinity of open water. Specifically, the *neighborhood*of an offshore pixel was defined as containing the 8 other pixels in the 3 x 3 box centered on the offshore pixel; the *neighborhood* of a near-shore pixel was defined as containing the 24 other pixels in the 5 x 5 box centered on the near-shore pixel; and the *neighborhood* of a shore pixel was defined as containing the 48 other pixels in the 7 x 7 box centered on the shore pixel. At any time when the neighborhood of an offshore, near-shore, or shore pixel contains three or more open-water pixels (sea ice concentration less than 15 percent), then the calculated sea ice concentration at the offshore, near-shore, or shore pixel is reduced by the value for that pixel in the matrix CMIN. Wherever the subtraction leads to negative sea ice concentrations, the concentrations are set to 0 percent. This land-spillover correction algorithm is clearly a rough approximation, as the contaminated amount does not stay constant over time; but the scheme has been found to reduce substantially the spurious sea ice concentrations on the grids.

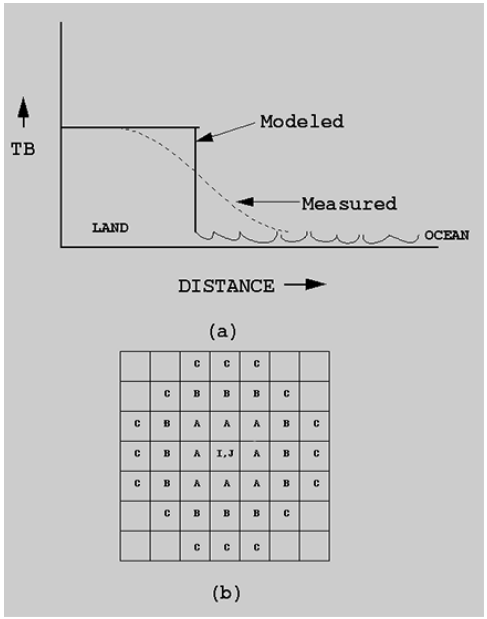

Figure 1. (a) Effect of the coarse resolution of the microwave antenna on a coastline resulting in false sea ice signals in the vicinity of the coast. (b) Seven-by-seven array used in the procedure to reduce the land-to-ocean spillover effect.

2.4.2.2 Residual Weather-Related Effects

Weather effects can cause the passive microwave signature of seawater to appear like that of ice (Cavalieri, 1995). A correction is made for removing spurious ice resulting from residual weather effects that were missed by the automatic weather filters. These valid ice masks are based on monthly climatological Sea Surface Temperatures (SSTs) from the NOAA Ocean Atlas (Levitus and Boyer, 1994). These data, originally on a two-degree by two-degree grid, were remapped onto the SSM/I grid. Because the SST data did not extend to the SSM/I coastline, the data were extrapolated to the coastline once they were mapped onto the SSM/I grid. The SST maps are used as follows:

- In the Northern Hemisphere, in any pixel where the monthly SST is greater than 278 K, the sea ice concentration is set to zero throughout the month.
- In the Southern Hemisphere, in any pixel where the monthly SST is greater than 275 K, the sea ice concentration is set to zero throughout the month.
- The higher threshold SST value was needed in the Northern Hemisphere because the 275 K isotherm used in the south was too close to the sea ice edge in the north. In a few instances, corrections to the regridded SST data were needed, because otherwise actual sea ice was being lost.

Figure 2a shows a sample sea ice concentration field without the land-spillover and residual weather correction, and Figure 2b shows that same sample after the correction is applied.

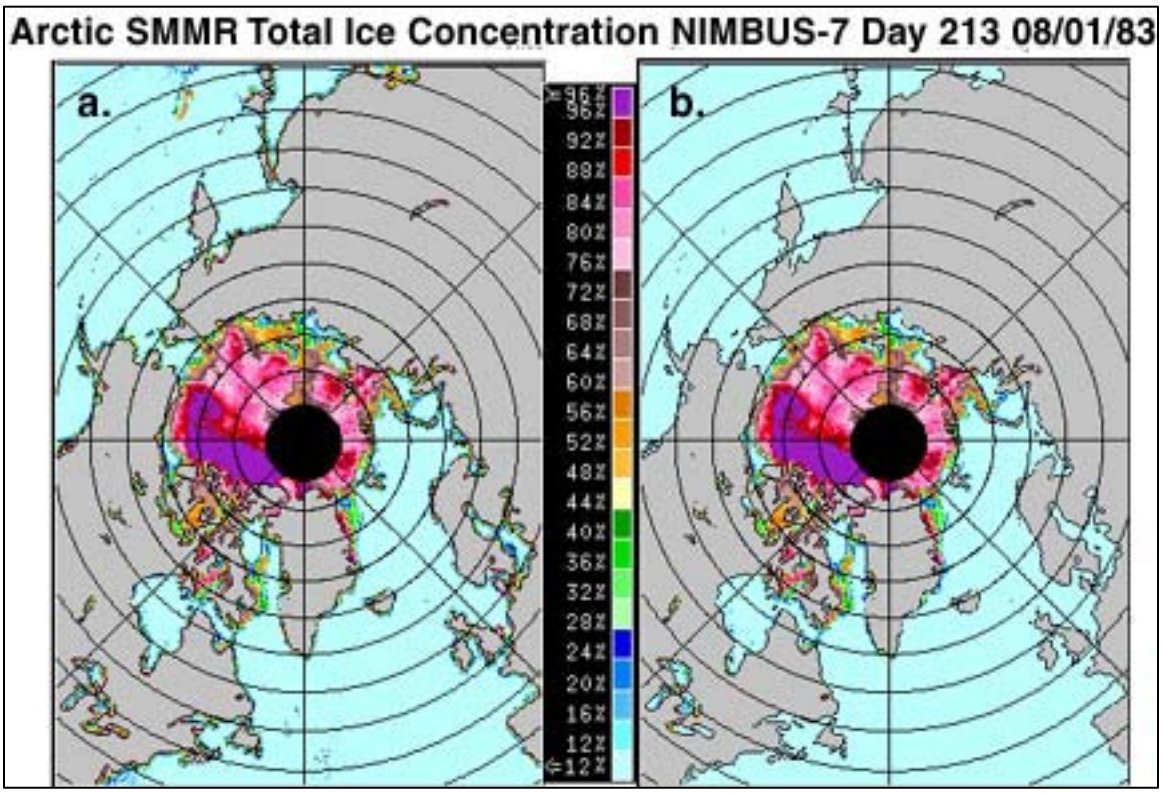

Figure 2. (a) Sea Ice Concentration Map of the Arctic for 01 August 1983 before the Application of the Land-spillover and Residual Weather Corrections (b) After Corrections

2.4.3 Manual Quality Control

The automated residual weather removal procedures unfortunately do not remove all spurious ice. In the older data in particular, clearly erroneous sea ice concentration values occurred on occasion due to bad input brightness temperatures, sometimes even with entire scans or swaths being dominated by bad data. Consequently, a manual quality control procedure was used to remove these erroneous data. This is done by visual inspection of the ice concentration images. In some instances, the erroneous nature of the data is quite clear, while in other instances it is less definitive. In the latter cases, a decision to retain or remove the suspect data is made based on consistency or lack of consistency with the data for the preceding and succeeding days. For data deemed to be spurious in the open ocean region, the ice concentrations are zeroed out. Data deemed to be erroneous within the ice cover are flagged as missing data and are filled like other data gaps, as described below.

2.4.4 Filling Data Gaps

There are instances of missing data. In some cases, whole days (or weeks or months) are missing. In other cases, large swaths or wedges of missing data exist within an image, along with scattered pixels of missing data throughout the grid. The scattered pixels of missing data, resulting generally

from mapping the orbital data to the SSM/I grid, were filled by applying a spatial linear interpolation scheme on the brightness temperature maps. The larger areas of missing data, resulting from gaps between orbital swaths (generally at low latitudes on daily maps) or from partial coverage or missing days, were filled by temporal interpolation on the sea ice concentration maps. No data at all were available for the period from 02 December 1987 through 12 January 1988. This gap was not filled by temporal linear interpolation; instead, it was left as missing data.

2.4.5 Monthly Data Generation

Once daily data have been processed as previously described, monthly data are generated. Monthly averaged sea ice concentration grids are produced from an average of the daily sea ice concentration grids available for each month. Monthly files for both hemispheres are provided for every month beginning October 1978. However, for October 1978, December 1987 and January 1988, the time series was incomplete: only three days of data were available during October 1978 to generate the monthly mean, only two days were available for December 1987, and only 19 days were available for January 1988. Therefore, the monthly means for these months do not represent the "true" monthly means.

In most cases, GSFC used all daily data to compute monthly averaged sea ice concentrations from a particular instrument until the data were no longer available. For example, SMMR data were used to compute monthly sea ice concentrations until the instrument stopped collecting data on 20 August 1987. Beginning 21 August 1987, SSM/I data were used. In 1991, DMSP-F8 SSM/I data were used through December 18; beginning December 19, DMSP-F11 SSM/I data were used.

Note: It is recommended that sea ice extent and area be computed from daily maps of ice concentrations that are then used to compute monthly averages of those parameters. Computations of sea ice extents and sea ice areas should not be made from the monthly-averaged ice concentration maps because that may result in a biased time series.

2.5 Quality, Errors, and Limitations

2.5.1 Data Validation by Source

The performance of the NASA Team algorithm was assessed in numerous studies such as Cavalieri et al. (1992), and these results apply to this data set. However, improvements in this data set that differ from previous studies include the minimization of coastal and open-ocean influences that tend to yield inaccurate sea ice concentrations. Visual data checking was used to assess the performance of these modifications.

2.5.2 Confidence Level/Accuracy Judgment

Estimates of the accuracy of the NASA Team algorithm vary depending on sea ice conditions, methods, and locations used in individual studies. Cavalieri et al. (1992) summarizes several of these studies. In general, accuracy of total sea ice concentration is within +/- 5 percent of the actual sea ice concentration in winter, and +/- 15 percent in the Arctic during summer when melt ponds are present on the sea ice. Accuracy tends to be best within the consolidated ice pack when the sea ice is relatively thick (greater than 20 cm) and ice concentration is high. Accuracy decreases as the proportion of thin ice increases. See Cavalieri et al. (1991), Cavalieri et al. (1992), Ivanova et al. (2014), Maslanik (1992), Meier (2005), Steffen et al. (1992), Steffen & Schwieger (1991), and Svendsen et al. (1983) for an overview of the algorithm performance.

2.5.3 Data Verification by Data Center

NSIDC staff visually checks the data files and selected graphics files. This includes verification of proper file structure; comparisons to existing SMMR-, SSM/I-, and SSMIS-derived sea ice concentration grids, masks, and information files; and examination of data quality.

Some weather-related effects and land contamination are still present. The amount and spatial distribution of remaining weather effects vary with season. Also, occasional bad scan lines still appear in the data. Based on NSIDC analyses, some sensor-to-sensor differences are likely to remain in these data, particularly for marginal ice zones. See NSIDC Special Report 5: An Intercomparison of DMSP F11- and F13-derived Sea Ice Products (Stroeve et al., 1997) for summaries of differences among the SSM/I sensors.

Residual weather effects and processing errors in May 1986 data result in large bands of very low ice concentrations over the open ocean in the Weddell, Bellingshausen, and Amundsen seas in the Southern Hemisphere. Although the magnitude of these false ice concentrations is less than one percent, users should be aware that such errors do occur in data for many days within that month.

Overlap periods exist when transitioning from one instrument to the next. These overlaps are from SMMR to DMSP-F8 SSM/I, from DMSP-F8 to -F11 SSM/I, from DMSP-F11 to -F13 SSM/I, and from DMSP-F13 SSM/I to DMSP-F17 SSMIS. During overlap periods, data were available from two instruments, although good data may not be available from both instruments during the entire operating overlap. Differences in ice covered area and ice extent during the overlap periods were minimized by tuning the sea ice algorithms. Wavelet analysis of the time series of ice extent and ice covered area show no significant offsets between the different satellites.

Tables 9 and 10 summarize the comparison between the ice covered areas and ice extent during the overlap periods, including mean differences and linear regression results of ice covered areas and ice extent. Mean differences are computed for SMMR minus DMSP-F8 SSM/I, DMSP-F8

SSM/I minus DMSP-F11 SSM/I, DMSP-F11 SSM/I minus DMSP-F13 SSM/I, and DMSP-F13 SSM/I minus DMSP-F17 SSMIS. Regression coefficients are computed using y = a0 + a1*x, for each (x, y) pair (x=SMMR, y=DMSP-F8 SSM/I); (x=DMSP-F8 SSM/I, y=DMSP-F11 SSM/I); (x=DMSP-F11 SSM/I, y=DMSP-F13 SSM/I); and (x=DMSP-F13 SSM/I, y=DMSP-F17 SSMIS). While this analysis shows no significant differences between the overall summaries of ice covered area and ice extent, significant regional differences in ice concentration may still be present.

Table 9. Northern Hemisphere Sensor Differences

	Mean Difference ($x\ 10^6 km^2$)	**Standard Deviation ($x\ 10^6 km^2$)**	**a_0 ($x\ 10^6$)**	**a_1 ($x\ 10^6$)**	**Correlation Coefficient**	**% Difference**
SMMR to DMSP-F8 SSM/I						
Ice area	0.073	0.054	0.214	0.947	0.999	1.34%
Ice extent	0.055	0.096	0.412	0.941	0.998	0.70%
DMSP-F8 to DMSP-F11 SSM/I						
Ice area	-0.019	0.036	0.955	0.914	0.996	0.18%
Ice extent	0.002	0.058	0.351	0.972	0.983	0.01%
DMSP-F11 to DMSP-F13 SSM/I						
Ice area	-0.0112	0.0296	0.0079	0.997	0.999	0.18%
Ice extent	-0.0004	0.0457	0.0199	0.997	0.999	-0.01%
DMSP-F13 to DMSP-F17 SSMIS						
Ice area	-0.0389	0.0188	0.0329	1.0007	0.999	0.5433%
Ice extent	-0.0027	0.0426	-0.0297	1.0032	0.999	-0.0156%

Table 10. Sothern Hemisphere Sensor Differences

	Mean Difference ($x\ 10^6 km^2$)	**Standard Deviation ($x\ 10^6 km^2$)**	**a_0 ($x\ 10^6$)**	**a_1 ($x\ 10^6$)**	**Correlation Coefficient**	**% Difference**
SMMR to DMSP-F8 SSM/I						
Ice area	0.018	0.072	0.225	0.982	0.992	0.15%
Ice extent	0.005	0.058	-0.198	1.011	0.998	0.0%
DMSP-F8 to DMSP-F11 SSM/I						
Ice area	-0.038	0.092	0.630	0.924	0.996	0.49%
Ice extent	0.012	0.067	0.289	0.974	0.998	0.08%

	Mean Difference ($x\ 10^6 km^2$)	Standard Deviation ($x\ 10^6 km^2$)	a_0 ($x\ 10^6$)	a_1 ($x\ 10^6$)	Correlation Coefficient	% Difference
DMSP-F11 to DMSP-F13 SSM/I						
Ice area	0.0311	0.0344	-0.0474	1.007	0.999	0.26%
Ice extent	0.0126	0.0402	-0.0186	1.002	0.999	0.08%
DMSP-F13 to DMSP-F17 SSMIS						
Ice area	-0.0212	0.0314	-0.0097	1.0034	0.999	0.1550%
Ice extent	-0.0009	0.0309	0.0109	0.9992	0.999	0.0304%

2.5.4 File Errors

Table 11 describes files that have been found to contain errors and that have been corrected during the life of this data set along with the types of errors that were corrected. NSIDC recommends data users download the corrected files for these dates listed in Table 11.

Table 11. Description of Corrected Files

File Date	File Name	Type of Correction	Date Correction was Made
1984-09	`nt_198409_n07_v01_n.bin`	Geolocation error	July 2014
1984-14-09	`nt_19840914_n07_v01_n.bin`	Geolocation error	July 2014
1983-07-30	`nt_19830730_n07_v01_n.bin`	Weather correction	January 2013
1984-07-26	`nt_19840726_n07_v01_n.bin`	Weather correction	January 2013
1984-07-28	`nt_19840728_n07_v01_n.bin`	Weather correction	January 2013
1984-07-30	`nt_19840730_n07_v01_n.bin`	Weather correction	January 2013
1985-07-01	`nt_19850701_n07_v01_n.bin`	Coastal/weather correction	January 2013
1985-07	`nt_198507_n07_v01_n.bin`	Coastal/weather correction	January 2013
1987-07-21	`nt_19870721_f08_v01_n.bin`	Weather correction	January 2013

File Date	File Name	Type of Correction	Date Correction was Made
1987-12-01	nt_19871201_f08_v01_n.bin	Ambiguous; not a clear source of error	January 2013
1987-12-01	nt_19871201_f08_v01_s.bin	Ambiguous; not a clear source of error	January 2013
1995-11-02	nt_19951102_f13_v01_n.bin	Ambiguous; not a clear source of error	January 2013
1995-11-14	nt_19951114_f13_v01_n.bin	Ambiguous; not a clear source of error	January 2013
1995-11	nt_199511_f13_v01_n.bin	Ambiguous; not a clear source of error	January 2013
1995-12-07	nt_19951207_f13_v01_n.bin	Land/coastal correction	January 2013
1996-04-10	nt_19960410_f13_v01_n.bin	Land/coastal correction	January 2013
1996-04-23	nt_19960423_f13_v01_n.bin	Land/coastal correction	January 2013
1996-05-09	nt_19960509_f13_v01_s.bin	Land/coastal correction	January 2013
1996-05	nt_199605_f13_v01_s.bin	Land/coastal correction	January 2013
1996-06-12	nt_19960612_f13_v01_n.bin	Land/coastal correction	January 2013
1996-06-18	nt_19960618_f13_v01_n.bin	Land/coastal correction; same pixels as 1996-06-12	January 2013
1996-06-19	nt_19960619_f13_v01_n.bin	Ambiguous; not a clear source of error	January 2013
1996-06-20	nt_19960620_f13_v01_n.bin	Land/coastal correction	January 2013
1996-06	nt_199606_f13_v01_n.bin	Land/coastal correction	January 2013
1996-10-06	nt_19961006_f13_v01_s.bin	Land/coastal correction	January 2013
1996-10	nt_199610_f13_v01_s.bin	Land/coastal correction	January 2013
1996-11-01	nt_19961101_f13_v01_n.bin	Land/coastal correction	January 2013
1996-11-06	nt_19961106_f13_v01_n.bin	Land/coastal correction	January 2013
1996-11-14	nt_19961114_f13_v01_n.bin	Ambiguous; not a clear source of error	January 2013

File Date	File Name	Type of Correction	Date Correction was Made
1996-12-05	nt_19961205_f13_v01_n.bin	Land/coastal correction; same pixels as 1996-06-12	January 2013
1996-12-23	nt_19961223_f13_v01_n.bin	Land/coastal correction; same pixels as 1996-06-12	January 2013

2.5.5 Sea Ice Pixel Correction

Additional Quality Control (QC) of the data set was done from 1978 to 2014 to remove additional spurious ice. Figures 3 and 4 show the number of pixels that are different across the time series due to the additional QC.

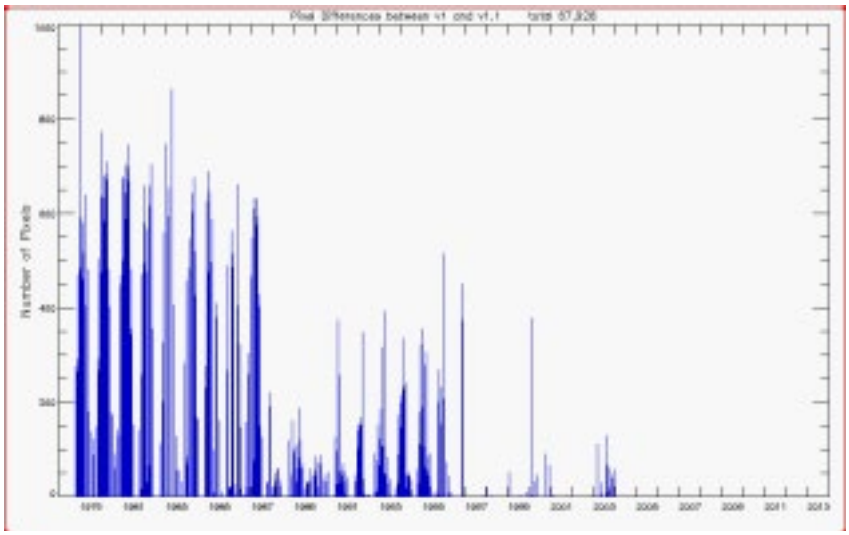

Figure 3. Number of Pixels that are Different Across the Time Series for the Northern Hemisphere

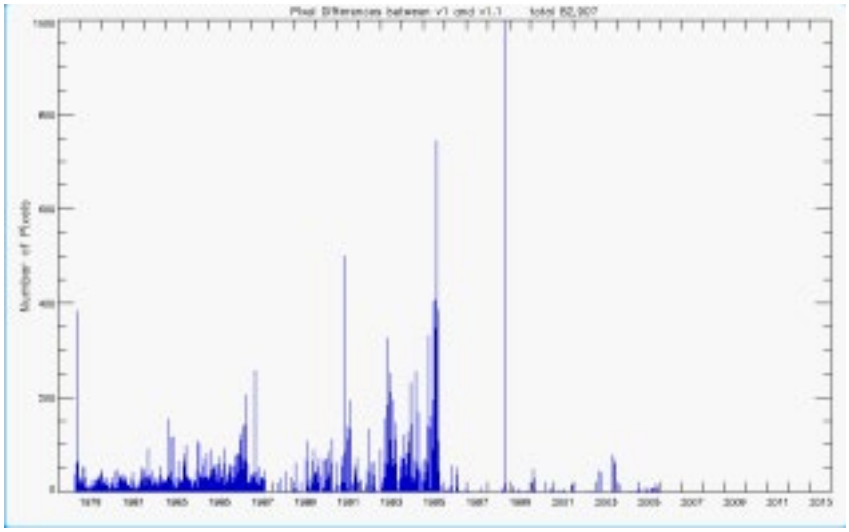

Figure 4. Number of Pixels that are Different Across the Time Series for the Southern Hemisphere

2.6 Instrumentation

2.6.1 Description

The SMMR is a 10-channel instrument delivering orthogonally polarized antenna temperature data at five dual-polarized (horizontal, vertical) frequencies: 6.6 GHz, 10.7 GHz, 18.0 GHz, 21.0 GHz, and 37.0 GHz.

The SSM/I is a seven-channel, orthogonally polarized, passive-microwave radiometric system. The instrument measures combined atmosphere and surface radiances at 19.3 GHz, 22.2 GHz, 37.0 GHz and 85.5 GHz frequencies.

The SSMIS sensor is a conically-scanning passive microwave radiometer that harnesses the imaging and sounding capabilities of three previous DMSP microwave sensors, including the SSMI, the SSM/T-1 temperature sounder, and the SSMI/T-2 moisture sounder. The SSMIS sensor measures microwave energy at 24 frequencies from 19 to 183 GHz with a swath width of 1700 km. Tables 12 and 13 give the FOV of each instrument.

Table 12. SSM/I and SSMIS FOV

Frequency	Footprint Size
19.3 GHz	70x45 km
22.2 GHz	60x40 km
37.0 GHz	38x30 km

Table 13. SMMR FOV

Frequency	Footprint Size
6.6 GHz	148x95 km
10.7 GHz	91x59 km
18.0 GHz	55x41 km
21.0 GHz	46x30 km
37.0 GHz	27x18 km

For more details regarding the SMMR, SSM/I, and SSMIS sensors, please refer to the SMMR, SSM/I, and SSMIS Sensors Summary.

2.6.2 Trajectory and Attitude

The Nimbus-7 and DMSP F-series spacecraft fly in near-polar sun-synchronous orbits; details their respective orbits are compared in Table 14.

Table 14. Comparison of Orbital Parameters

Parameter	Nimbus-7	DMSP-F8	DMSP-F11	DMSP-F13	DMSP-F17
Nominal Altitude[1]	955 km	860 km	830 km	850 km	850 km
Inclination Angle	99.1 degrees	98.8 degrees	98.8 degrees	98.8 degrees	98.8 degrees
Orbital Period	104 minutes	102 minutes	101 minutes	102 minutes	102 minutes
Ascending Node Equatorial Crossing (Local Time)	Approx. 12:00 p.m.	Approx. 6:00 a.m.	Approx. 5:00 p.m.	Approx. 5:43 p.m.	Approx. 5:31 p.m.
Algorithm Frequencies[1]	18.0, 37.0 GHz	19.3, 37.0 GHz	19.3, 37.0 GHz	19.3, 37.0 GHz	19.3, 37.0 GHz
Earth Incidence Angle[1]	50.2	53.1	52.8	53.4	53.1
3 dB Beam Width (Degrees)[1]	1.6, 0.8	1.9, 1.1	1.9, 1.1	1.9, 1.1	1.9, 1.1
[1] Indicates sensor and spacecraft orbital characteristics of the sensors used in generating the sea ice concentrations.					

3 SOFTWARE AND TOOLS

Software tools are available via the Polar Stereographic web page. Software includes IDL routines to ingest and read sea ice concentration data. Masks and overlays are also provided.

Table 15 lists the tools that can be used with this data set. For a comprehensive list of all polar stereographic tools and for more information, see the Polar Stereographic web page.

Table 15. Tools for this Data Set

Tool Type	Tool File Name(s) or Description
Data Extraction	`extract_ice.pro`

Geocoordinate	`locate.for`
	`mapll.for and mapxy.for`
	`psn25lats_v3.dat and pss25lats_v3.dat`
	`psn25lons_v3.dat and pss25lons_v3.dat`

Pixel-Area	`psn25area_v3.dat and pss25area_v3.dat`

Land Masks	`gsfc_25n.msk and gsfc_25s.msk`
	`coast_25n.msk and coast_25s.msk`
	`ltln_25n.msk and ltln_25s.msk`
	`pole_n.msk`

Region Masks	`region_n.msk and region_s.msk`

Tool Type	Tool File Name(s) or Description
Ocean Masks	Includes monthly ocean masks and maximum extent masks for the Northern (n) and Southern (s) Hemispheres

4 VERSION HISTORY

Table 16 summarizes the Version history for this product.

Table 16. Processing History

Version	Date	Description
V1.1	December 2015	Data were reprocessed from 1978 to 2014, and additional QC of the data set was done to remove additional spurious ice. Refer to Figure 3 and Figure 4, which show the number of pixels that are different across the time series due to the additional QC. In addition, the data set no longer includes overlap dates during satellite transition periods. Refer to Table 13 for the time periods of each satellite used in this data set. This version also extends the temporal coverage through the present.
V1	March 2015	SSMIS pole hole mask replaces SSM/I pole hole mask for all data from 01 January 2008 to present.
V1	July 2014	An error was found in the sea ice concentration field for 14 September 1984. Due to a geolocation error in the source data, several hundred thousand square kilometers of erroneous ice occurred in that data. The original file has been removed and replaced with an average of the two files nearest in time (September 12 and 16). The monthly September 1984 average concentration field was reprocessed using the replaced September 14 data. See Table 12 for the file names and the correction made.
V1	June 2014	The browse images for the entire record have been reprocessed to include a title and simplified color bar; the data were not affected.
V1	January 2013	NSIDC applied corrections to 29 files that showed errors in a previous release of these data. The errors occurred in files from both SMMR (1983 – 1985) and SSM/I (1995 – 1996). See Table 12 for a list of these files.
V1	January 1996	Original version of data.

5 RELATED DATA COLLECTIONS

Near-Real-Time DMSP SSM/I-SSMIS Daily Polar Gridded Sea Ice Concentrations

Bootstrap Sea Ice Concentrations from Nimbus-7 SMMR and DMSP SSM/I

Sea Ice Index

Sea Ice Trends and Climatologies from SMMR and SSM/I-SSMIS

Sea Ice Remote Sensing (Cryospheric Sciences) at NASA Goddard Space Flight Center

6 ACKNOWLEDGMENTS

Walt Meier, Florence Fetterer, Ken Knowles, Matt Savoie, Mary Jo Brodzik
National Snow and Ice Data Center (NSIDC)
Boulder, Colorado USA

7 REFERENCES

Andersen, S., R. Tonboe, L. Kaleschke, G. Heygster, and L. T. Pedersen. 2007. Intercomparison of passive microwave sea ice concentration retrievals over the high-concentration Arctic sea ice, *J. Geophys. Res*., 112, C08004, https://doi.org/10.1029/2006JC003543.

Cavalieri, D. J., J. Crawford, M. Drinkwater, W. J. Emery, D. T. Eppler, L. D. Farmer, M. Goodberlet, R. Jentz, A. Milman, C. Morris, R. Onstott, A. Schweiger, R. Shuchman, K. Steffen, C. T. Swift, C. Wackerman, and R. L. Weaver. 1992. *NASA Sea Ice Validation Program for the DMSP SSM/I: Final Report.* NASA Technical Memorandum 104559. National Aeronautics and Space Administration, Washington, D. C. 126 pages. https://ntrs.nasa.gov/citations/19920015007.

Cavalieri, D. J., J. Crawford, M. R. Drinkwater, D. Eppler, L. D. Farmer, R. R. Jentz and C. C. Wackerman. 1991. Aircraft Active and Passive Microwave Validation of Sea Ice Concentration from the DMSP SSM/I. *Journal of Geophysical Research* 96(C12):21,989-22,009, https://doi.org/10.1029/91JC02335.

Cavalieri, D. J., K. M. St. Germain, and C. T. Swift. 1995. Reduction of Weather Effects in the Calculation of Sea Ice Concentration with the DMSP SSM/I. *Journal of Glaciology*. 41(139):455-464, https://doi.org/10.3189/S0022143000034791.

Cavalieri, D. J., and C. L. Parkinson, 2012: Arctic sea ice variability and trends, 1979-2010, *The Cryosphere*, 6, 881-889, https://doi.org/10.5194/tc-6-881-2012.

Cavalieri, D. J., C. l. Parkinson, P. Gloersen, J. C. Comiso, and H. J. Zwally. 1999. Deriving Long-term Time Series of Sea Ice Cover from Satellite Passive-Microwave Multisensor Data Sets. *Journal of Geophysical Research* 104(7): 15,803-15,814, https://doi.org/10.1029/1999JC900081.

Cavalieri, D. J., C. l. Parkinson, P. Gloersen, and H. J. Zwally. 1997. *Arctic and Antarctic Sea Ice Concentrations from Multichannel Passive-microwave Satellite Data Sets: October 1978 to*

December 1996, User's Guide. NASA Technical Memorandum 104647. 17 pages. (see PDF).

Gloersen P. and D. J. Cavalieri. 1986. Reduction of Weather Effects in the Calculation of Sea Ice Concentration from Microwave Radiances. *Journal of Geophysical Research* 91(C3):3913-3919, https://doi.org/10.1029/JC091iC03p03913.

Gloersen P., W. J. Campbell, D. J. Cavalieri, J. C. Comiso, C. L. Parkinson, H. J. Zwally. 1992. *Arctic and Antarctic Sea Ice, 1978-1987: Satellite Passive Microwave Observations and Analysis.* NASA Special Publication 511, https://ntrs.nasa.gov/citations/19940012966.

Ivanova, N., O. M. Johannessen, L. T. Pedersen, and R. T. Tonboe. 2014. Retrieval of Arctic sea ice parameters by satellite passive microwave sensors: A comparison of eleven sea ice concentration algorithms, *IEEE Trans. Geosci. Rem. Sens*., 52(11), 7233-7246, https://doi.org/10.1109/TGRS.2014.2310136.

Levitus, S. and Boyer, T. P. 1994. World Ocean Atlas 1994, Volume 4: Temperature, NOAA National Oceanographic Data Center, Ocean Climate Laboratory, U.S. Department of Commerce, Washington D.C., https://repository.library.noaa.gov/view/noaa/1381.

Martino, M. G., D. J. Cavalieri, P. Gloersen, and H. J. Zwally. 1995. *An Improved Land Mask for the SSM/I Grid*. Edited by J. G. Acker. NASA Technical Memorandum 104625. 9 pages. (See PDF).

Maslanik, J. A. 1992. Effects of Weather on the Retrieval of Sea Ice Concentration and Ice Type from Passive Microwave Data. *International Journal of Remote Sensing*13(1):37-54, https://doi.org/10.1080/01431169208904024.

Meier, W. N. 2005. Comparison of passive microwave ice concentration algorithm retrievals with AVHRR imagery in the Arctic peripheral seas, IEEE *Trans. Geosci. Rem. Sens*., 43(6), 1324-1337, https://doi.org/10.1109/TGRS.2005.846151.

Parkinson, C. l., J. C. Comiso, H. J. Zwally, D. J. Cavalieri, P. Gloersen, and W. J. Campbell. 1987. *Arctic Sea Ice, 1973-1976: Satellite Passive-Microwave Observations,*NASA SP-489, National Aeronautics and Space Administration, Washington, D. C. 296 pages, https://ntrs.nasa.gov/citations/19870015437.

Steffen, K. and A. Schwieger. 1991. NASA Team Algorithm for Sea Ice Concentration Retrieval from Defense Meteorological Satellite Program Special Sensor Microwave/Imager: Comparison with Landsat satellite imagery. *Journal of Geophysical Research* 96(C12):21,971-21,988, https://doi.org/10.1029/91JC02334.

Steffen, K., D. J. Cavalieri, J. C. Comiso, K. St. Germain, P. Gloersen, J. Key, and I. Rubinstein. 1992. The Estimation of Geophysical Parameters Using Passive Microwave Algorithms. Chapt 10 In *Microwave remote sensing of sea ice.* Frank Carsey, editor. American Geophysical Union. Washington, D. C. 243-259, https://doi.org/10.1029/GM068p0201.

Stroeve, J., X. Li, and J. Maslanik. 1997. NSIDC Special Report 5: An Intercomparison of DMSP F11- and F13-derived Sea Ice Products. Boulder, CO: National Snow and Ice Data Center. (PDF)

Svendsen, E., K. Kloster, B. Farrelly, O. M. Johannessen, J. A. Johannessen, W. J. Campbell, P. Gloersen, D. Cavalieri, and C. Matzler. 1983. Norwegian Remote Sensing Experiment: Evaluation of the Nimbus-7 Scanning Multichannel Microwave Radiometer for Sea Ice Research. *Journal of Geophysical Research* 88(C5):2781-2791, https://doi.org/10.1029/JC088iC05p02781.

8 DOCUMENT INFORMATION

8.1 Publication Date

March 2019

8.2 Date Last Updated

February 2023